Modeling Tree Effects on Path Loss in a Residential Environment

Saúl A. Torrico, *Member, IEEE*, Henry L. Bertoni, *Fellow, IEEE*, and Roger H. Lang, *Fellow, IEEE*

***Abstract*— A theoretical model is proposed to compute the path loss in a vegetated residential environment, with particular application to mobile radio systems. As in the past, the row of houses or blocks of buildings are viewed as diffracting cylinders lying on the earth and the canopy of the trees are located adjacent to and above the houses/buildings. In this approach, a row of houses or buildings is represented by an absorbing screen and the adjacent canopy of trees by a partially absorbing phase screen. The phase-screen properties are found by finding the mean field in the canopy of the tree. Physical optics (PO) is then used to evaluate the diffracting field at the receiver level by using a multiple Kirchhoff–Huygens integration for each absorbing/phase half-screen combination.**

***Index Terms*—Propagation, urban areas, vegetation.**

I. Introduction

MOTIVATED by the development of cellular systems, personal communications systems (PCS), and wireless local loop systems (WLL), there is a need to better understand the propagation channel. This work describes an approach to predict the propagation loss between a base-station transmitter and a mobile receiver in a vegetated residential area. A residential area is defined as an area outside the high-rise core of a city where the heights of the buildings or houses are of relatively uniform height. A residential area may also have trees whose canopies are adjacent to and above the buildings or houses. A PCS or WLL system is expected to have the base-station transmitters located close to the surrounding rooftops so that the propagation takes place over the rooftops. Theoretical models allow precise quantitative descriptions of a residential environment in terms of parameters such as the building heights, street widths, and type of trees in contrast to the ambiguous nature of more conventional empirical models [1].

A theoretical model is proposed to include the effects of trees as well as houses or buildings on the propagation loss in residential areas. As in past models [2], [3], the row of houses or blocks of buildings are viewed as diffracting cylinders lying on the earth and the canopy of the trees are located adjacent to and above the houses/buildings. In this approach, a row of houses or buildings is represented by an absorbing screen and the adjacent canopy of trees by a partially absorbing phase screen [3]. The field at the aperture of the first absorbing screen depends on the mean field going through the first tree due to an incident plane wave. Physical optics (PO) is then used to evaluate the diffracting field at each of the successive absorbing/phase half-screens configuration up to the mobile receiver by using the multiple Kirchhoff–Huygens integration. In order to find the properties of a partially absorbing phase screen such as the mean field, the attenuation, and phase delay, trees are represented as an ensemble of leaves and branches all having prescribed location and orientation statistics. Leaves are modeled as flat, circular, lossy-dielectric discs and branches as finitely long, circular, lossy-dielectric cylinders. The mean field in the canopy is calculated using the discrete scattering theory of Foldy and Lax [4]–[6]. By solving the wave equation for the mean scattered field propagating through a tree, it is found that the wave propagation constant has both real and imaginary components. The integrated effect of the propagation constant over the tree volume leads to expressions for the attenuation and phase delay of the partially absorbing phase screen. As it has been shown in [3], in a residential environment the overall path loss depends very much on the real and imaginary parts of the tree propagation constant. Finally, the shape of the cylinder of tree crowns is modeled as an ellipse.

Following this approach, results are presented to characterize the effects of trees on the propagation loss in residential environments for different grazing incident angles as well as different separation distances between absorbing/phase screens.

II. Tree Modeling

To find the mean field, the attenuation, and the phase delay of a partially absorbing phase screen, trees are modeled as discrete random ensemble of leaves and branches all having prescribed orientation and location statistics. Because of the randomness associated within the medium of discrete scatters, the wave behavior in a tree is better represented by a modern stochastic model [4]–[6]; this provides the basis for computing the mean field and the propagation constant. The integrated effect of the propagation constant over the tree volume leads to expressions for the attenuation and phase delay of a partially absorbing screen.

The model was first developed by Foldy [4] and later extended by Lax [5], Twersky [6], Lang [7], and Chauhan *et al*. [8]. Consider the canopy of a tree as a layer of thickness d, which is modeled by a slab of leaves and branches (as shown in Fig. 1). The leaves are modeled as randomly positioned flat-

Manuscript received March 25, 1997; revised January 20, 1998.

S. A. Torrico is with Comsearch, Reston, VA 22091 USA.

H. L. Bertoni is with the Center for Advanced Technology in Telecommunications, Polytechnic University, Brooklyn, NY 11201 USA.

R. H. Lang is with the Department of Electrical Engineering and Computer Science, George Washington University, Washington, DC 20052 USA.

Publisher Item Identifier S 0018-926X(98)04876-5.

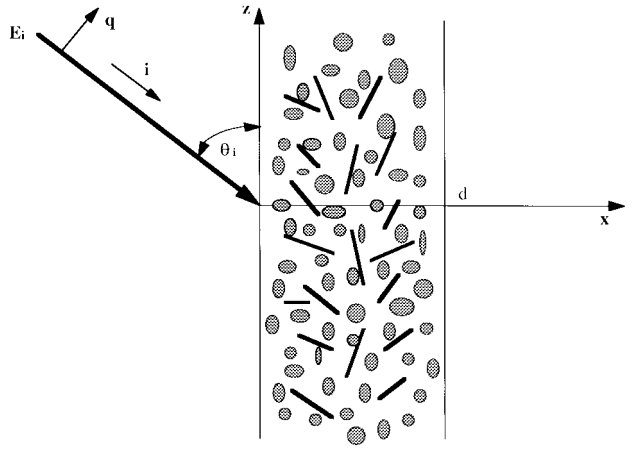

Fig. 1. Incident plane wave on slab with thin discs and thin cylinders.

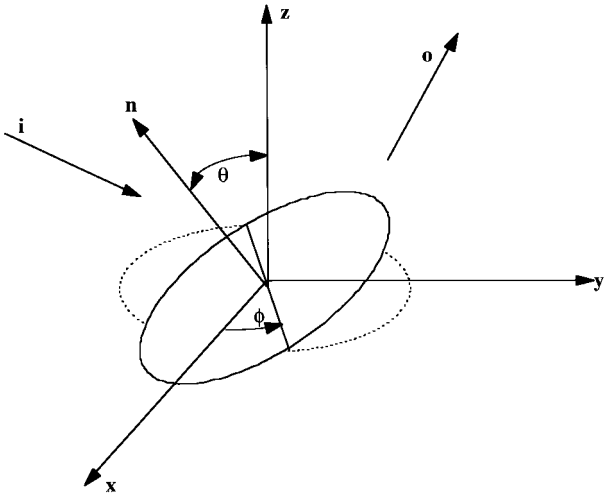

Fig. 2. Leaf (thin-disc) orientation with respect to the slab.

circular lossy-dielectric discs and the branches as randomly positioned finitely long lossy-dielectric cylinders. It is assumed that the thin cylinders and the flat circular disc are distributed uniformly in azimuthal coordinates ϕ. The probability densities for the azimuthal coordinates and the polar coordinates are independent for the leaves as well as for the branches. Here, the azimuthal angle ϕ is defined in the plane perpendicular to the slab. As shown in Fig. 1, we have three-layered medium with free-space for $x < 0$ and $x > d$ having a free-space permeability μ_0 and permittivity ϵ_0. In the region $0 < x < d$, we consider identical discs with a constant volume density ρ_d and identical cylinders with a constant volume density ρ_c within the slab of width d. Each disc or cylinder has its volume V_p and dielectric constant ε_r. A free-space background medium is assumed in the slab. The interface between the slab and free-space is considered smooth—not introducing any reflections.

The calculation of the mean field in the canopy is obtained by determining the dyadic scattering amplitudes of an arbitrarily oriented thin disc and of an arbitrarily oriented thin cylinder.

A. Scattering Amplitude—Thin Disc

Assume that a plane wave of unit amplitude and polarization $\hat{\mathbf{q}}$ (hatted quantities are unit vectors) is incident upon the disc

$$\mathbf{E_i}(\mathbf{x}, \hat{\mathbf{q}}) = \hat{\mathbf{q}} e^{ik_0(\hat{\mathbf{i}}\cdot\mathbf{x})} \tag{1}$$

where $\hat{\mathbf{i}}$ is the direction of propagation and k_0 is the free-space propagation constant. The disc is assumed to have cross-sectional shape S, a radius a, a thickness t, and a complex relative permittivity ε_r throughout the disc. As is shown in Fig. 2, the orientation of the disc is defined by the angle θ with respect to the z axis and the angle ϕ with respect to the x axis.

From the radiation condition, the vector scattered amplitude $\mathbf{f}$, as observed in direction $\hat{\mathbf{o}}$, can be related to the total electric field $\mathbf{E}_{\text{ind}}$ induced within the disc [9] as follows:

$$\mathbf{f}(\hat{\mathbf{o}}, \hat{\mathbf{i}}, \hat{\mathbf{q}}) = \frac{k_o^2 \chi_r}{4\pi}(\bar{\mathbf{I}} - \hat{\mathbf{o}}\,\hat{\mathbf{o}}) \cdot \int_V \mathbf{dx'} \mathbf{E}_{\text{ind}}(\mathbf{x'}, \hat{\mathbf{q}}) e^{-ik_o(\hat{\mathbf{o}}\cdot\mathbf{x'})} \tag{2}$$

where $\chi_r = \varepsilon_r - 1$ is the susceptibility of the disc, $\bar{\mathbf{I}}$ is a unit dyadic, and V is the volume of the disc. The induced field in the disc can be found when the disc radius a is much greater than the thickness of the disc t and the disc is electrically thin $k_{\text{disc}} t \ll 1$, where $k_{\text{disc}} = k_o\sqrt{|\varepsilon_r|}$. Here, the induced field within the disc may be approximated by the electric field in an unbounded slab having the same orientation as the disc. Under this approximation, the electromagnetic boundary condition requiring the continuity of the tangential field components across an arbitrary interface can be employed to show that the induced electric field within the disc is given by

$$\mathbf{E}_{\text{ind}}(\mathbf{x'}, \hat{\mathbf{q}}) = \left[\hat{\mathbf{q}} - (\hat{\mathbf{n}}\cdot\hat{\mathbf{q}})\hat{\mathbf{n}} + \frac{1}{\varepsilon_r}(\hat{\mathbf{q}}\cdot\hat{\mathbf{n}})\hat{\mathbf{n}}\right] e^{ik_o(\hat{\mathbf{i}}\cdot\mathbf{x'})} \tag{3}$$

where $\hat{\mathbf{n}}$ is the unit vector normal to the disc (as shown in Fig. 2). Finally, the vector scattering amplitude is obtained by substituting (3) into (2) and assuming that there is no-phase variation in the induced field normal to the disc ($k_{\text{disc}} t \ll 1$) and that the wavelength is greater than the radius of the disc ($\lambda \gg a$), we find that

$$\mathbf{f}(\hat{\mathbf{o}}, \hat{\mathbf{i}}, \hat{\mathbf{q}}) = \chi_r t \left(\frac{k_o a}{2}\right)^2 (\bar{\mathbf{I}} - \hat{\mathbf{o}}\,\hat{\mathbf{o}}) \cdot \left[\hat{\mathbf{q}} - \left(\frac{\chi_r}{1+\chi_r}\right)(\hat{\mathbf{n}}\cdot\hat{\mathbf{q}})\hat{\mathbf{n}}\right]. \tag{4}$$

Note that the scalar scattering amplitude f_{pq} can be obtained by

$$f_{pq} = \hat{\mathbf{p}} \cdot \hat{\mathbf{f}}(\hat{\mathbf{o}}, \hat{\mathbf{i}}, \hat{\mathbf{q}}) \tag{5}$$

where $\hat{\mathbf{p}}$ is the scattering polarization in direction $\hat{\mathbf{o}}$.

B. Scattering Amplitude—Thin Cylinder

Consider a plane wave as (1) to be incident upon a cylinder of radius a, length l, and complex relative permittivity ε_r . As is shown in Fig. 3, the cylinder axis is inclined by an angle θ from the z axis and by an azimuthal angle ϕ from the x axis.

To find the vector scattering amplitude $\mathbf{f}$ using (2), we need to find the induced electric field within the cylinder. The

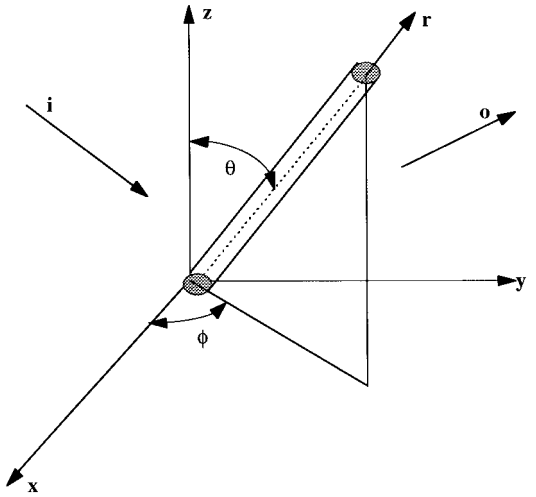

Fig. 3. Branch (thin-cylinder) orientation with respect to the slab.

induced field within the cylinder is found by using quasi-static techniques. Under this approximation, the electromagnetic boundary condition requiring the continuity of the tangential field components across an arbitrary interface can be employed to show that the induced electric field within the cylinder is given by

$$\mathbf{E}_{\text{ind}}(\mathbf{x}', \hat{\mathbf{q}}) = \left[\frac{2}{\varepsilon_r + 1}\hat{\mathbf{q}} + \left(\frac{\varepsilon_r - 1}{\varepsilon_r + 1}\right)(\hat{\mathbf{q}} \cdot \hat{\mathbf{r}})\hat{\mathbf{r}}\right] e^{ik_o(\bar{\mathbf{x}} \cdot \hat{\mathbf{i}})} \quad (6)$$

where $\hat{\mathbf{r}}$ is a unit vector directed along the cylinder axis as shown in Fig. 3. Finally, the vector scattering amplitude is obtained by substituting (6) into (2), to obtain

$$\mathbf{f}(\hat{\mathbf{o}}, \hat{\mathbf{i}}, \hat{\mathbf{q}}) = l\left(\frac{k_o a}{2}\right)^2 \chi_r(\bar{\mathbf{I}} - \hat{\mathbf{o}}\,\hat{\mathbf{o}}) \cdot \left[\frac{2}{\chi_r + 2}\hat{\mathbf{q}} + \frac{\chi_r}{\chi_r + 2}(\hat{\mathbf{q}} \cdot \hat{\mathbf{r}})\hat{\mathbf{r}}\right] \quad (7)$$

where $\chi_r = \varepsilon_r - 1$ is the susceptibility of the cylinder and $\bar{\mathbf{I}}$ is a unit dyadic.

C. Mean Field

The mean field in the canopy is derived by using the multiple scattering theory of Foldy–Lax [4], [5]. The Foldy [4] approximation assumes that the total field incident on a scatterer is equal to the mean field. This approximation requires that the fractional volume occupied by the scatters be small in comparison to the total volume V of the canopy. The vector wave equation for the mean field in the canopy is given by [7]

$$\bar{\mathbf{L}} \cdot \langle \mathbf{E}(\mathbf{x}) \rangle = \mathbf{g}(\mathbf{x}) + \int_v \mathbf{ds}\rho(\mathbf{s}) \times \int \mathbf{dx}' \langle \bar{\mathbf{t}}(\mathbf{x} - \mathbf{s}, \mathbf{x}' - \mathbf{s}) \rangle \cdot \langle \mathbf{E}(\mathbf{x}') \rangle \quad (8)$$

where $\bar{\mathbf{L}} = \nabla \times \nabla \times \bar{\mathbf{I}} - k_0^2 \bar{\mathbf{I}}$, $\rho(\mathbf{s})$ is the density of particles at $\mathbf{s}$, and $\mathbf{g}(\mathbf{x})$ is equal to $i\omega\mu_0 \mathbf{J}(\mathbf{x})$ where $\mathbf{J}(\mathbf{x})$ is the source current density and μ_0 is the free-space permeability. Also, $\langle \bar{\mathbf{t}}(\mathbf{x} - \mathbf{s}, \mathbf{x}' - \mathbf{s}) \rangle$ is the dyadic transition operator of a particle located at $\mathbf{s}$ where the brackets means the average angular dependence. The transition operator is related to the scattering amplitude as shown in [7]. It should be noted that (8) differs from the vector Helmholtz equation only because of the added integral term arising as a result of the scatterers. The first term of the right side of the equation is due to the source; if we assume plane wave incidence then this term is equal to zero. The second term on the right side of (8) is due to the scatterers and is zero if there are no scatterers in the medium.

Now, consider a plane wave of unit amplitude and polarization $\hat{\mathbf{q}}$ is incident on the slab of scatters in the direction $\hat{\mathbf{i}}$, as in (1). The incident plane wave makes an angle of θ_i with respect to the z axis, as shown in Fig. 1. The mean field in the canopy is obtained by solving the vector wave equation (8) and can be written as

$$\langle \mathbf{E}(x, z; \hat{\mathbf{q}}) \rangle = \hat{\mathbf{q}} e^{i\kappa x - ik_0 \cos(\theta_i) z} \quad (9)$$

where

$$\kappa = k_0 \sin(\theta_i) + \frac{2\pi}{k_0 \sin(\theta_i)} \sum_t \rho_t \langle f_{qq}^{(t)}(\hat{\mathbf{i}}, \hat{\mathbf{i}}) \rangle. \quad (10)$$

Here, κ is the propagation constant in the x direction of polarization $\hat{\mathbf{q}}$. $\langle f_{qq}^{(t)}(\hat{\mathbf{i}}, \hat{\mathbf{i}}) \rangle$ is the mean forward scattering amplitude over the scatterers orientation and the sum is over scatterer type t. The solution reveals that to a first approximation, the scattering amplitude is obtained in the forward direction, and because of the assumed independence of the distribution $\rho(\mathbf{s})$ on the transverse coordinates, the mean field in the canopy behaves like a plane wave in the transverse coordinates. It is important to mention that the propagation constant cannot be calculated to a higher accuracy than to the first order, since the mean equation in the medium has also been found to this accuracy. The mean forward-scattering amplitude can be written as

$$\langle f_{qq}^{(t)}(\hat{\mathbf{i}}, \hat{\mathbf{i}}) \rangle = \frac{1}{2\pi} \int d\theta f_{\rho q}^{(t)}(\hat{\mathbf{i}}, \hat{\mathbf{i}}) p(\theta) \quad (11)$$

where $p(\theta)$ is the probability density function of the inclination angle and it is assumed that the probability density of the azimuthal angle is uniformly distributed from 0 to 2π. Because of the assumed azimuthal symmetry of the scatterers, the mean wave of the vertical and horizontal polarizations do not couple so that no depolarization effects occur at the level of the mean wave.

In general, the wave propagation constant in the canopy κ has a real and imaginary component. This results from the fact that the scatterers have loss. The imaginary part of κ gives the specific attenuation in nepers per meter or alternatively in dB per meter and is given by

$$\alpha_{\text{dB/m}} \approx 8.686\ \text{Img}(\kappa). \quad (12)$$

The implication of the fact that the scatterers have loss is that the mean field in the canopy decays in its respective direction of propagation. A measure of this decay is the skin depth d_s in meters defined by

$$d_s = \frac{1}{\text{Img}(\kappa)}. \quad (13)$$

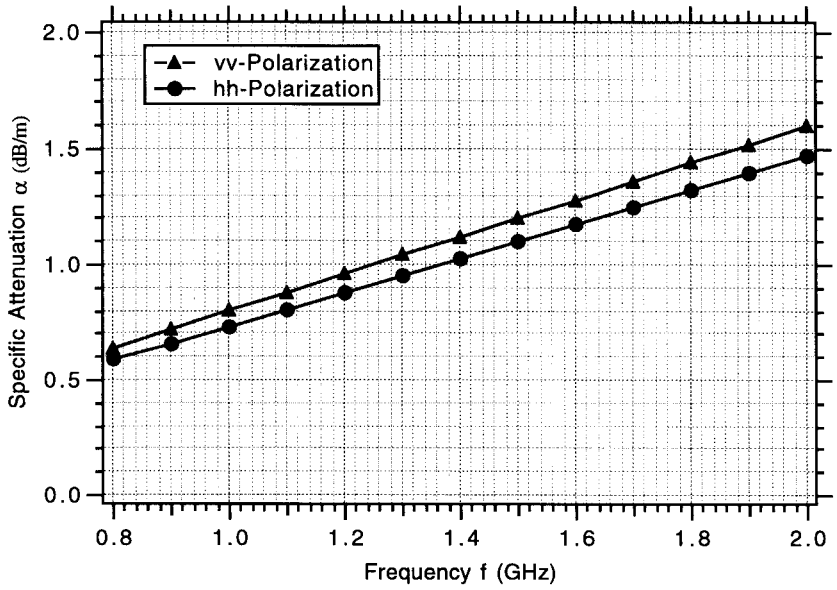

Fig. 4. Calculated tree-specific attenuation versus frequency for a 90° incident plane wave.

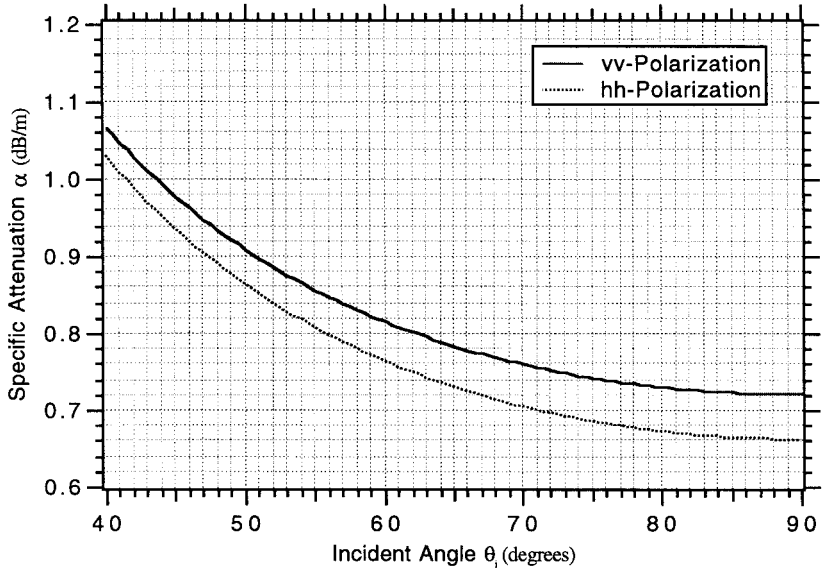

Fig. 5. Calculated tree-specific attenuation versus incident angle for an incident plane wave at 900 MHz.

The importance of the skin depth is that whenever the thickness of the slab is less than the skin depth we only need to consider the mean fields; otherwise, we may need to consider the mean fields as well as the incoherent fields. In this analysis, it is assumed that the incoherent field is small compared to the mean field, therefore, it has been disregarded.

D. Numerical Results

The numerical calculation of the specific attenuation and the skin depth of a tree is given in this section. The procedure is to specify the disc and cylinder parameters including their respectively probability density distributions of the inclination angle θ and the azimuthal angle ϕ. The specific attenuation α and the skin depth d_s are calculated for different frequencies and for different incident angles. The leaves are assumed to have a radius $a = 5$ cm and a thickness $t = 0.5$ mm, a dielectric constant of $\varepsilon_r = 26 + i7$ [10], and a density of $\rho_1 = 350/\text{m}^3$. The branches are assumed to have a radius $a = 1.6$ cm and a branch length $l = 50$ cm, a dielectric constant $\varepsilon_r = 20 + i7$, and a density $\rho_b = 2/\text{m}^3$. The probability density for the leaves and the branches in the azimuthal coordinate ϕ is assumed to be uniformly distributed from 0° to 360°. The probability density in the θ coordinate is dependent on vegetation type. For the branches and the leaves it is considered to be uniformly distributed

$$p_\theta(\theta) = \frac{1}{\theta_2 - \theta_1} \tag{14}$$

where for the leaves, $\theta_2 = 180°$ and $\theta_1 = 0°$ and for the branches $\theta_2 = 60°$ and $\theta_1 = 0°$. Finally, it is important to note that the relative dielectric constants of the leaves and branches

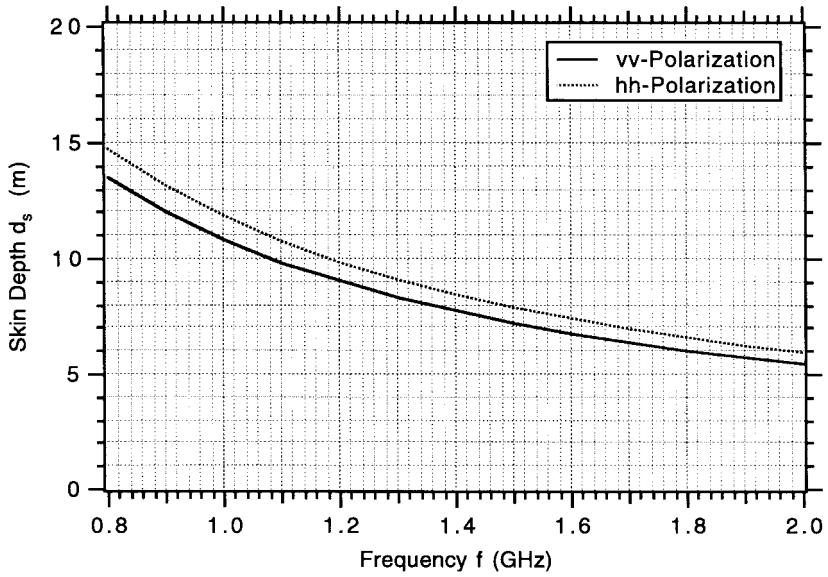

Fig. 6. Calculated skin depth versus frequency for a 90° incident plane wave.

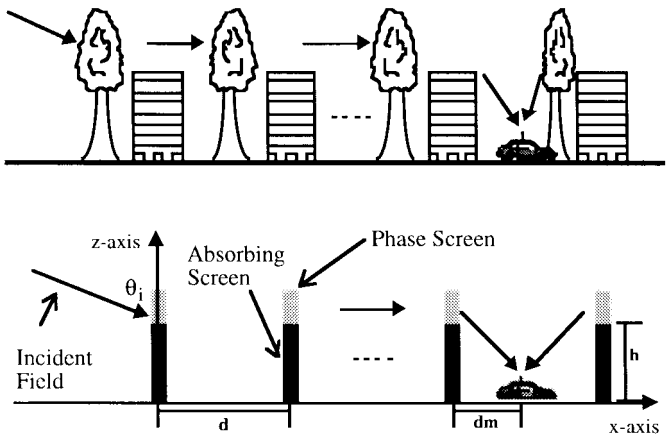

Fig. 7. Row of houses and row of trees with its equivalent geometry.

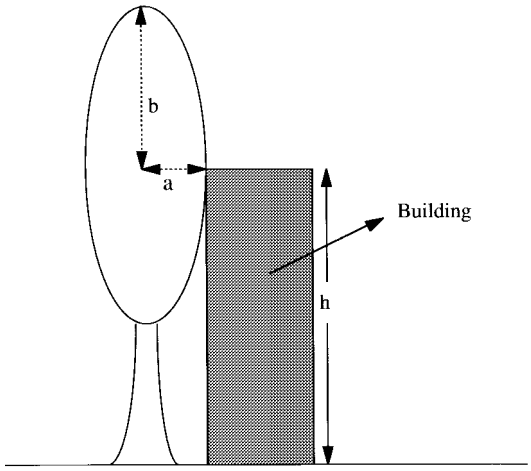

Fig. 8. Geometry for a single elliptical tree/building configuration.

are frequency dependent [10]. In our analysis constant values for the permittivities of the leaves and the branches have been assumed, because the permittivities of the leaves and the branches do not change much between 800–2000 MHz.

Fig. 4 shows a plot of tree-specific attenuation versus frequency for both incident polarizations. It is seen that the specific attenuation for vertically polarized waves is higher than for horizontal polarization. The reason lies in the statistical distribution of leaves and branches in reference to the angle of incidence θ_i of the plane wave. In Fig. 5, we plot the specific attenuation of a tree versus the angle the incident plane wave makes with the slab interface for both polarizations. It is observed that for incident angles between 80° and 90°, the specific attenuation changes very little.

Fig. 6 shows a plot of skin depth versus frequency for both polarizations for $\theta_i = 90°$. The importance of the skin depth is that whenever the thickness of the tree is less than the skin depth we only need to consider the mean fields; otherwise, we may have to consider the incoherent field as well as the mean field.

III. Multiple Buildings and Trees Formulation

Extending the method of Walfisch and Bertoni [2], a theoretical approach is introduced to account for trees in the propagation loss in residential areas. As in the past model [2], [3], a row of houses or block of buildings is viewed as a diffracting cylinder lying on the earth, with the canopy of a row of trees located adjacent to and above the buildings. Because of the small grazing angle between the incident field and the rooftops of the buildings, the buildings are modeled as perfect absorbing screens and the trees, which are adjacent to and above the buildings, are modeled as partially absorbing phase screens. The properties of a partially absorbing phase screen were derived in Section II.

PO is used to compute the fields diffracted by a series of absorbing/phase screens, as shown in Fig. 7. The absorbing/phase screens lie in the x-z plane, the height of the absorbing screens above the x axis is h, the separation distance between screens is d, the origin coincides with the first screen, and the phase screens are located above

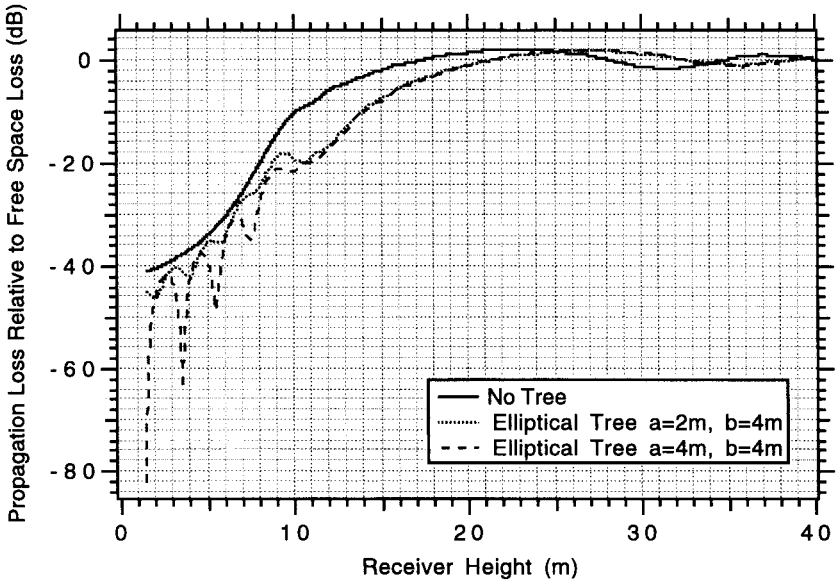

Fig. 9. Calculated height gain curves for 20 buildings/trees at the mobile receiver, for a 90° incident plane wave, and 50-m distance separation between buildings/trees at 900 MHz.

and to the left of the absorbing screens. The method used to find the field in successive apertures is based on the multiple Kirchhoff–Huygens integrations. The mean field in the aperture of the first absorbing/phase screen configuration is assumed to be that of a unit-amplitude time-harmonic $\exp(-i\omega t)$ plane wave with polarization $\hat{\mathbf{q}}$ and incident angle θ_i as in (1), multiplied by a factor giving the attenuation and phase delay of the mean field as a result of going through the first phase screen that is located adjacent to and above the first absorbing screen. The mean field incident on the aperture of any other absorbing/phase screen is found by integrating over the previous aperture the product of the mean field illuminating the previous aperture, the change in the mean field as a result of going through the phase screen, and the far-field two-dimensional free-space Green's function. This process is repeated up to the mobile receiver. Thus, the mean field $\langle E_{n+1}(x,z)\rangle$ in the aperture of the $n+1$ absorbing/phase screen or at the location of the mobile receiver, where $n \in \{1, N\}$ and N is the number of absorbing/phase screens can be found from

$$\langle E_{n+1}(x,z)\rangle = -\frac{k_{x0}}{2}\sqrt{\frac{2}{\pi k_0}}e^{-i\frac{\pi}{4}}\int_h^\infty \langle E'_n(x',z')\rangle \frac{e^{ik_0\rho}}{\sqrt{\rho}}\,dz' \tag{15}$$

where $\langle E'_n(x',z')\rangle$ is the mean field at the aperture of the previous n absorbing/phase screen and is given by

$$\langle E'_n(x',z')\rangle = e^{iw(z')(\kappa-k_{x0})}\langle E_n(x',z')\rangle. \tag{16}$$

Here, $w(z')$ is the width of a tree at different heights above the absorbing screen, κ is the propagation constant in the tree given by (10), and

$$\rho = \sqrt{(x-x')^2+(z-z')^2}. \tag{17}$$

We note from (16), that the mean field $\langle E'_n(x',z')\rangle$ at the aperture of the n absorbing/phase screen is composed of two terms; the first term is the phase change and attenuation due to the tree and the second term is the field incident on the aperture n. The effect of phase change due to propagation through the trees is like that of a lens where focusing can occur. The imaginary part of κ causes attenuation of the signal.

In general, the integral of the mean field $\langle E_{n+1}(x,z)\rangle$ cannot be carried out in a closed form and we must resort to numerical techniques, keeping in mind the need for reasonable accuracy and realistic computational time. In developing a numerical approach as in [2], it is necessary to convert the continuous integration into a sum of terms, where each term represents an approximation to the integral over a small interval. The mean field given in (15) is rewritten as

$$\langle E_{n+1}(x,z)\rangle = \int_h^\infty A_n(x',z')e^{i\phi(x',z')}\,dz' \tag{18}$$

where

$$A_n(x',z') = -\frac{k_{x0}}{2}\sqrt{\frac{2}{\pi k_0}}\frac{e^{-i\frac{\pi}{4}}}{\sqrt{\rho}}\langle E'_n(x',z')\rangle e^{ik_{z0}z'} \tag{19}$$

and

$$\phi(x',z') = -k_{z0}z' + k_0\rho \tag{20}$$

with $k_{z0} = k_0\cos\theta_i$. In order to evaluate the mean field (18) numerically, we convert the continuous integral into a sum of terms, where each term represents an approximation to the integral over a small interval. First, we divide the integration aperture into M intervals of $\Delta z'$ such that the mean field in the (x,z) plane on the $n+1$ aperture or at the mobile receiver is given by

$$\langle E_{n+1}(x,z)\rangle = \sum_{m=0}^{m=M}\Delta\langle E'_n(x',z')\rangle \tag{21}$$

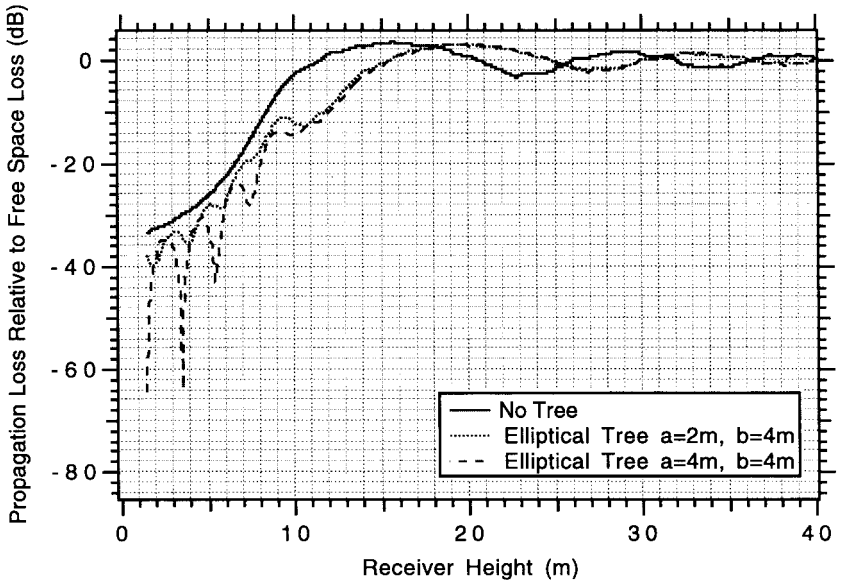

Fig. 10. Calculated height gain curves for 20 buildings/trees at the mobile receiver, for an 89.5° incident plane wave, and 50-m distance separation between buildings/trees at 900 MHz.

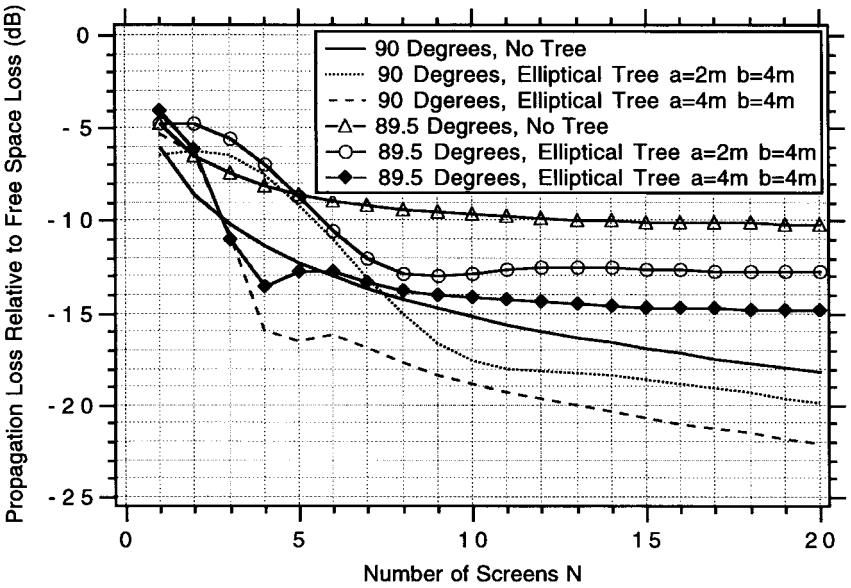

Fig. 11. Propagation loss relative to free-space loss at the top of the absorbing screens versus number of screens for a incident plane wave of different incident angles and 50-m distance separation between buildings/trees at 900 MHz.

where

$$\Delta\langle E_n'(x',z')\rangle = \int_{z_m'}^{z_{m+1}'} A_n(x',z')e^{i\phi(x',z')}\,dz' \qquad (22)$$

and

$$z_m' = m\Delta z' + h.$$

Then, by using the first two terms of a Taylor series expansion for $A_n(x',z')$ and for $\phi(x',z')$ and integrating over the interval $m\Delta z' < z' < (m+1)\Delta z'$ in a closed form, we find the solution of the mean field $\langle E_{n+1}(x,z)\rangle$.

In addition, the sum in (21) must be finite, which means that the field must be artificially limited in the z axis. However, an abrupt truncation of the field will result in strong reflections from the nonphysical upper boundary. A practical approach to this problem is to add an absorbing region above the maximum altitude of interest [11] where the field is attenuated smoothly to zero. In the calculations we have used a Hamming window in the absorbing region.

A. Numerical Results

In the previous sections, expressions were derived for the field incident on a mobile receiver or on successive absorbing edges. The numerical calculations of the propagation loss relative to free-space loss is given in this section. The canopy of the trees is modeled as having an elliptical shape, with a minor axis equal to a and a major axis equal to b. The minor axis of the ellipse is parallel with the x axis and the major axis is parallel to the z axis. The elliptical shapes of the tree canopies have their centers at the tops of the buildings and

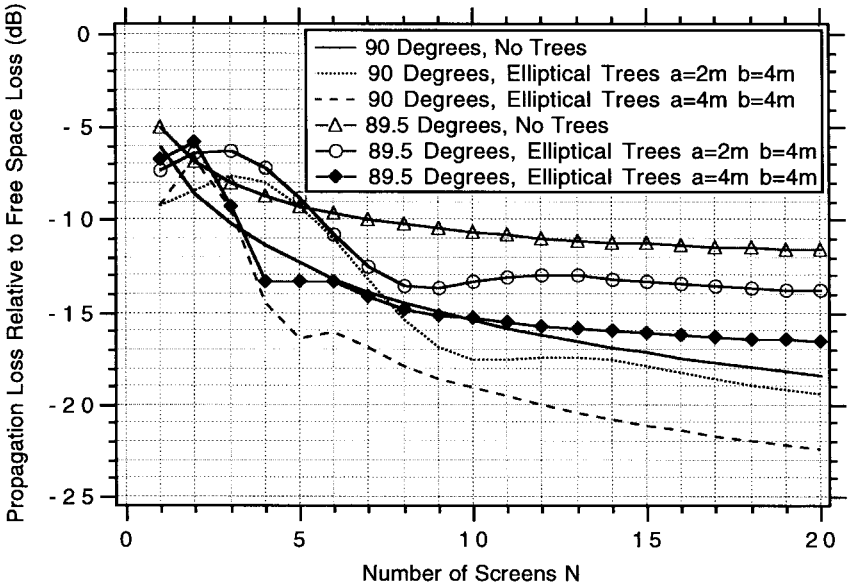

Fig. 12. Propagation loss relative to free-space loss at the top of the absorbing screens versus number of screens for a incident plane wave of different incident angles and 33-m distance separation between buildings/trees at 900 MHz.

are located a meters to the left of the buildings; the heights of the trees are b meters above the buildings as shown in Fig. 8. The electrical characteristics of a tree are given in Section II. The buildings have a height of 8 m, a separation distance between buildings of 50 m, and a 20 m distance separation between the last building and the mobile receiver as shown in Fig. 7. All the results that follow are based on an incident plane wave of unit amplitude at 900 MHz. Throughout the numerical calculations, it is assumed that the propagation constant of the trees does not change with the tree heights.

In Fig. 9, we plot the propagation loss relative to free-space loss as a function of height at the mobile receiver after 20 rows of buildings (solid line), after 20 rows of buildings/trees with tree canopy dimensions $a = 4$ m and $b = 4$ m (dashed line) and after 20 rows of buildings/trees with tree canopy dimensions $a = 2$ m and $b = 4$ m (dotted line). For these calculations, the plane wave was taken to be propagating along the x axis ($\theta_i = 90°$). The corresponding results for an oblique plane wave ($\theta_i = 89.5°$) are shown in Fig. 10. It is observed that both figures show the interference patterns for different sizes of trees in the shadow region of the last building/tree configuration. Note, that as we double the width of the trees the interference pattern in the shadow region gets more severe, because the effects of trees on the propagation loss is like that of a lens where focusing and defocusing effects occur. Comparing Figs. 9 and 10, we see that by changing the incident angle of the incident plane wave, we shift each of the curves, but not by the same amount.

Figs. 11 and 12 show the propagation loss relative to free-space loss at the top of successive buildings with and without trees. The results in Fig. 11 are for the same geometry used to obtain the results in Figs. 9 and 10, whereas the results in Fig. 12 were obtained assuming $d = 33$ m instead of 50 m. For the oblique plane wave ($\theta_i = 89.5°$), after 10 rows the fields at the tops of the buildings vary by less than 1 dB. As is to be expected, for incidence along the x axis ($\theta_i = 90°$) the fields continue to decrease with N. This behavior is similar to that found previously for buildings alone. After ten rows the wider trees are seen to give 4–5 dB more path loss than the buildings by themselves.

IV. Conclusion

A theoretical model has been developed to compute the path loss in a vegetated residential environment for mobile applications. The model shows the effects of trees on the propagation loss and identifies those physical properties of the trees that are significant in computing their propagation constant. These properties include the probability density functions of the scatterers, the electrical characteristics of the scatterers, and the dimensions of the scatterers.

References

[1] Y. Okumura, E. Ohmori, T. Kawano, and K. Fukuda, "Field strength and its variability in VHF and UHF land-mobile radio service," *Rev. Elect. Commun. Lab.*, vol. 16, pp. 825–873, 1968.

[2] J. Walfisch and H. L. Bertoni, "A theoretical model of UHF propagation in urban environment," *IEEE Trans. Antenna Propagat.*, vol. 36, pp. 1788–1796, Dec. 1988.

[3] S. A. Torrico, H. L. Bertoni, and R. H. Lang, "Theoretical investigation of foliage effects on path loss for residential environments," in *Proc. IEEE Veh. Technol. Conf.*, pp. 854–858, 1996.

[4] L. L. Foldy, "The multiple scattering of waves," *Phys. Rev.*, vol. 67, no. 3, pp. 107–119, 1945.

[5] M. X. Lax, "Multiple scattering of waves," *Rev. Mod. Phys.*, vol. 23, no. 4, pp. 287–310, 1951.

[6] V. Twersky, "Multiple scattering of electromagnetic waves by arbitrary configurations," *J. Math. Phys.*, vol. 8, no. 3, pp. 589–610, 1967.

[7] R. H. Lang, "Electromagnetic backscattering from a sparse distribution of lossy dielectric scatterers," *Radio Sci.*, vol. 16, no. 1, pp. 15–30, 1981.

[8] N. S. Chauhan, R. H. Lang, and K. J. Ranson, "Radar modeling of a boreal forest," *IEEE Trans. Geosci. Remote Sensing*, vol. 29, pp. 627–638, July 1991.

[9] D. M. LeVine, R. Meneghini, R. H. Lang, and S. S. Seker, "Scattering from arbitrary oriented dielectric discs in the physical optics regime," *J. Opt. Soc. Amer.*, vol. 73, pp. 1255–1262, 1983.

[10] C. Matzler, "Microwave (1–100 GHz) dielectric model of leaves," *IEEE Trans. Geosci. Remote Sensing*, vol. 32, pp. 947–949, Sept. 1994.

[11] S. A. Torrico, "Wave propagation modeling in the troposphere using the Fourier split-step method," Master's thesis, George Washington Univ., Washington, DC, 1992.

Saúl A. Torrico (M'93) was born in Cochabamba, Bolivia. He received the B.S. and M.S. degrees in electrical engineering, in 1983 and 1992, respectively, and the Ph.D. degree in electrophysics in 1998, all from George Washington University, Washington DC.

Dr. Torrico joined Comsearch, Reston, VA, in 1985, where he is currently Senior Technical Consultant. Since 1985 he has been responsible for directing Comsearch's efforts in research and development in the areas of radio-wave propagation, system design for applications pertinent to mobile communications, microwave communications, and satellite communications systems. Between 1990 and 1992 he was selected as a Lead Engineer to develop a workstation-based microwave frequency management software package for a U.K. personal communication network (PCN) carrier as well as for a Germany cellular carrier. Since then, the software package has been considered a standard in Germany and is used in several European and Latin American countries to design personal communication system design and microwave systems. Between 1983 to 1985 he designed and implemented AM, FM, TV, and cellular systems. He teaches radio-wave propagation modeling and radio network planning for mobile systems. He has published articles on the topic of outdoor radio-wave propagation. His current research topics include wave propagation in natural and urban terrain, radiation and scattering, wave propagation in random media, and spectrum management techniques.

Dr. Torrico is a member of the IEEE Antenna and Propagation Society, the Vehicular Technology Society, and the Geoscience and Remote Sensing Society. He is a member of both the American Geophysical Union in Radio Science and the National Spectrum Management Association.

Henry L. Bertoni (M'67–SM'79–F'87), for photograph and biography, see this issue, p. 863.

Roger H. Lang (S'66–M'68–SM'86–F'89) received the B.S. and M.S. degrees in electrical engineering, in 1962 and 1964, respectively, and the Ph.D. degree in electrophysics, in 1968, all from the Polytechnic Institute of Brooklyn, NY.

From 1963 to 1964, he worked at Bell Telephone Laboratories, Murray Hill, NJ, on satellite antennas. From 1969 to 1970 he did postdoctoral work on wave propagation in random media at the Courant Institute of Mathematical Science, New York University, before joining George Washington University (GWU), Washington, DC. He is now a Professor in the Department of Electrical Engineering and Computer Science at GWU. From 1984 to 1988 he served as Department Chairman. He has worked with NASA's Land Processes Group in developing microwave discrete scattering models of vegetation.

Dr. Lang is an Associate Editor for the IEEE Geoscience and Remote Sensing Society Microwave Scattering and Propagation. He was co-chairman of the Technical Program Committee for the International Geoscience and Remote Sensing Symposium, College Park, MD, in 1990.